Proceedings of the ASME 2013 Summer Heat Transfer Conference
HT2013
July 14-19, 2013, Minneapolis, MN, USA

HT2013-17249

ANGULAR FALSE SCATTERING IN RADIATIVE HEAT TRANSFER ANALYSIS USING THE DISCRETE-ORDINATES METHOD WITH HIGHER-ORDER QUADRATURE SETS

Brian Hunter
Department of Mechanical and Aerospace Engineering,
Rutgers, The State University of New Jersey,
98 Brett Road, Piscataway, NJ 08854
brianhun@eden.rutgers.edu

Zhixiong Guo
Department of Mechanical and Aerospace Engineering,
Rutgers, The State University of New Jersey,
98 Brett Road, Piscataway, NJ 08854
guo@jove.rutgers.edu

ABSTRACT

The S_N quadrature set for the discrete-ordinates method is limited in overall discrete direction number in order to avoid physically unrealistic negative directional weight factors. Such a limitation can adversely impact radiative transfer predictions. Directional discretization results in errors due to ray effect, as well as angular false scattering error due to distortion of the scattering phase function. The use higher-order quadrature schemes in the discrete-ordinates method allows for improvement in discretization errors without an overall directional limitation. In this analysis, four higher-order quadrature sets (Legendre-Equal Weight, Legendre-Chebyshev, Triangle Tessellation, and Spherical Ring Approximation) are implemented for determination of radiative transfer in a 3-D cubic enclosure containing participating media. Radiative heat fluxes, calculated at low direction number, are compared to the S_N quadrature and Monte Carlo predictions to gauge quadrature accuracy. Additionally, investigation into the reduction of angular false scattering with sufficient increase in direction number using higher-order quadrature, including heat flux accuracy with respect to Monte Carlo and computational efficiency, is presented. While higher-order quadrature sets are found to effectively minimize angular false scattering error, it is found to be much more computationally efficient to implement proper phase function normalization for accurate radiative transfer predictions.

INTRODUCTION

One of the most commonly implemented approximate methods for determining radiative transfer through numerical solution of the Equation of Radiative Transfer (ERT) is the Discrete-Ordinates Method (DOM) [1-3], first proposed by Chandrasekhar [1] for atmospheric and astrophysical radiation, and later adapted to solve both the neutron-transport equation [4] and for use in radiative heat transfer. In many processes, such as high-temperature combustion and material processing [5-8] or biomedical therapeutic applications involving the interaction of ultrafast laser light with living tissue [9-13], radiation is the dominant mode of heat transfer, and thus complete and accurate ERT solutions are required for accurate physical modeling. In practical applications where light scattering exists, analytic solution of the ERT is extremely difficult, mandating the necessity for accurate yet efficient numerical solutions of the ERT.

Fiveland [14,15] and Truelove [16] were among the first to apply the DOM in the field of radiation, determining steady-state radiative transfer in both 2-D and 3-D enclosures containing participating media. Later, Guo and Kumar extended use of the DOM for accurate determination of ultrafast radiative transfer in participating media [17,18] through solution of the transient ERT. Further works by Guo and co-authors implemented the transient DOM (TDOM) to accurately and efficiently model short-pulsed irradiation of turbid media [12,13], laser-tissue welding and soldering [11], and pulse train irradiation using Duhamel's superposition theorem [6,19].

The DOM uses a finite set of discrete radiation directions, with corresponding directional weight factors, to approximate the continuous angular variation. Although the choice of discrete quadrature set is generally arbitrary, the directions must satisfy certain moment conditions [20]. The level-symmetric S_N quadrature [20,21] is one of the most commonly implemented quadrature sets, where the total number of directions is $M = N(N+2)$. This quadrature set, however, is limited in total discrete direction number, as the directional weighting factors become unrealistically negative for S_{20} and greater in order to satisfy the specific moment-matching criteria [21]. The DOM is known to suffer from ray effect [22] due to the inexact approximation of the continuous angular variation,

and so directional limitation constraints significantly restrict the adaptivity of the S_N quadrature.

In media, such as biological tissue, where light scattering is highly anisotropic, a poor approximation of the continuous angular variation results in a lack of system scattered energy conservation [23-25]. Correction of this error via traditional phase-function normalization techniques can result in significant distortion and alteration of the scattering phase function after directional discretization [25-28], an error recently classified as "angular false scattering" [27,28], or a second type of false scattering due to angular discretization. Angular false scattering should not be confused with the traditional "spatial false scattering" error, or numerical diffusion, which occurs due to imprecise space discretization [22]. A phase-function normalization technique recently developed by the current authors [26-30] implements an additional constraint to simultaneously conserve scattered energy and scattering asymmetry factor, and has been shown to accurately predict radiative transfer and effectively eliminate/minimize angular false scattering errors.

Since angular false scattering errors manifest solely due to angular discretization, a sufficient increase in discrete direction number may effectively minimize this error without additional normalization treatment. To analyze this hypothesis, higher-order quadrature sets with no inherent directional limitations are necessary. Several higher-order quadrature sets have been developed in recent years. The Legendre-Equal Weight (P_N-EW) and Legendre-Chebyshev (P_N-T_N) quadratures were developed by Longoni and Haghighat [31] using the Gauss-Legendre quadrature technique. Additionally, two purely geometric quadrature sets called the T_N triangle-tessellation quadrature [32] and the Spherical Ring Approximation ($SRAP_N$) [33] were developed to specifically address the directional limitation of traditional level-symmetric sets. A thorough analysis of the impact of directional increases on angular false scattering errors is crucial, as the necessity of implementing an artificial phase-function normalization procedure to produce accurate radiative transfer predictions may prove to be unnecessary.

In this study, the impact of higher-order quadrature sets for 3-D radiative transfer in highly anisotropic scattering media is examined. Radiative heat fluxes generated using higher-order quadratures are compared to both Monte Carlo solutions [25] and lower-order S_N results to gauge their accuracy. Distortions in heat flux profiles, due to angular false scattering after application of scattered energy normalization, are examined for all quadratures with increasing direction number. Additionally, application of Hunter and Guo's normalization technique is investigated in conjunction with higher-order quadrature application. Finally, the computational efficiency of DOM with higher-order quadratures is examined, and a final determination of the practicality of substantial increase in direction number over implementation of phase-function normalization is made.

NOMENCLATURE

$A^{l'l}$	Normalization coefficients
g	Asymmetry factor
I	Radiative intensity (W/m^2sr)
M	Total number of directions
$\boldsymbol{r}$	Position vector
$\hat{\boldsymbol{s}}$	Unit direction vector
w	Discrete direction weight

Greek Symbols

σ_a	Absorption coefficient (m^{-1})
σ_s	Scattering coefficient (m^{-1})
μ, η, ξ	Direction cosines
Φ	Scattering phase function
$\tilde{\Phi}$	Normalized scattering phase function
ϕ	Radiation direction azimuthal angle (°)
Θ	Scattering angle (°)
θ	Radiation direction polar angle (°)
ω	Scattering albedo, $= \sigma_s/(\sigma_a + \sigma_s)$

Subscripts

b	Blackbody
HG	Henyey-Greenstein
N	DOM Quadrature index

Superscripts

$'$	Radiation incident direction
l, l'	Radiation directions
$l'l$	From direction l' into direction l

DISCRETIZATION OF ERT

The steady-state ERT of radiation intensity I in a gray, absorbing-emitting and anisotropically scattering medium can be written as follows, using general vector notation:

$$\hat{\boldsymbol{s}} \cdot \nabla I(\boldsymbol{r}, \hat{\boldsymbol{s}}, t) = -(\sigma_a + \sigma_s) I(\boldsymbol{r}, \hat{\boldsymbol{s}}, t) + \sigma_a I_b(\boldsymbol{r}, t) + \frac{\sigma_s}{4\pi} \int_{4\pi} I(\boldsymbol{r}, \hat{\boldsymbol{s}}', t) \Phi(\hat{\boldsymbol{s}}', \hat{\boldsymbol{s}}) d\Omega' \quad (1)$$

In the preceding equation, the single term on the left-hand side represents the spatial gradients of radiative intensity. The three terms on the right-hand side represent intensity attenuation due to absorption and out-scattering, blackbody emission due to radiative intensity, and intensity augmentation due to radiative energy in-scattering, respectively.

For a 3-D enclosure defined by the Cartesian coordinate system, Eq. (1) can be expanded as a simultaneous set of partial differential equations in discrete directions $\hat{\boldsymbol{s}}^{\boldsymbol{l}}$ using the DOM, as follows:

$$\mu^l \frac{\partial I^l}{\partial x} + \eta^l \frac{\partial I^l}{\partial y} + \xi^l \frac{\partial I^l}{\partial z} = -(\sigma_a + \sigma_{sm}) I^l + S^l \tag{2a}$$

$$S^l = \sigma_a I_b + \frac{\sigma_s}{4\pi} \sum_{\substack{l'=1 \\ l' \neq l}}^{M} w^{l'} \Phi^{l'l} I^{l'} \tag{2b}$$

$$\sigma_{sm} = \sigma_s \left(1 - \frac{1}{4\pi} w^l \Phi^{ll}\right) \tag{2c}$$

where $l = 1,2,\dots,M$ (the total number of directions). The direction cosines $\mu = \sin\theta\cos\phi$, $\eta = \sin\theta\sin\phi$, and $\xi = \cos\theta$ correspond to the x-, y-, and z-directions, respectively, and θ and ϕ are the polar and azimuthal angles corresponding to radiation direction $\hat{\boldsymbol{s}}^{\boldsymbol{l}}$. Using traditional quadrature approximation, the in-scattering integral in the source term of Eq. (2b) has been replaced by a discrete summation. where $w^{l'}$ is the directional weighting factor corresponding to radiation direction $\hat{\boldsymbol{s}}^{\boldsymbol{l'}}$, and $\Phi^{l'l}$ is the diffuse scattering phase-function value between two arbitrary radiation directions $\hat{\boldsymbol{s}}^{\boldsymbol{l'}}$ and $\hat{\boldsymbol{s}}^{\boldsymbol{l}}$. Eq. (2c) defines a modified scattering coefficient σ_{sm} [34], in which forward-scattering is treated as transmission and extracted from the in-scattering summation. This treatment has been shown to improve DOM computational efficiency for radiative transfer in strongly-scattering media [34].

In general, the Mie scattering phase function Φ is a highly oscillatory function, which can be expressed as an infinite summation of Legendre polynomials. However, exact Mie phase function implementation can be difficult due to the oscillatory nature, and thus researchers commonly use phase-function approximations as a viable and efficient alternative. One phase-function approximation that has become popular in radiative transfer simulation involving highly anisotropic scattering media, due to its' ability to accurately capture strong-forward scattering peaks, is the Henyey-Greenstein (HG) phase-function approximation. The analytic form of the HG phase function is as follows:

$$\Phi_{HG}(\Theta) = \frac{1 - g^2}{[1 + g^2 - 2g\cos(\Theta)]^{1.5}} \tag{3}$$

where Θ is the 3-D scattering angle between radiation directions $\hat{\boldsymbol{s}}'$ and $\hat{\boldsymbol{s}}$, and the overall asymmetry factor g is a measure of the average cosine of scattering angle Θ.

To solve Eqs 2(a-c), the domain of interest is subdivided into numerous control volumes, while spatial gradients are approximated using traditional control-volume methods. Spatial grid sizes should be taken as small as possible to obtain sufficient solution accuracy while keeping in mind that considerable grid refinement can substantially increase computational complexity [34]. The quadrature scheme must be specified at the outset of the problem in order to fully define the angular distribution of the M discrete radiation directions. After defining both spatial and angular grids, as well as medium properties, Eqs. 2(a-c) can be solved via the DOM using a simple control-volume marching scheme [18], the details of which are not repeated here but are readily available both in standard text [3] and in the authors' previous publications [17,18].

HIGHER-ORDER QUADRATURE SCHEMES

The choice of quadrature set for the DOM is generally arbitrary, although quadrature sets are commonly developed around satisfaction of directional moment conditions [3]. After directional discretization, the m^{th}-order directional moment conditions can be expressed for the three direction cosines, as follows:

$$\begin{aligned} \frac{1}{4\pi}\sum_{l=1}^{M}(\mu^l)^m w^l = \frac{1}{4\pi}\sum_{l=1}^{M}(\eta^l)^m w^l = \frac{1}{4\pi}\sum_{l=1}^{M}(\xi^l)^m w^l \\ = \begin{cases} 0\,, & m = 1,3,5,7,\dots \\ \dfrac{1}{m+1}\,, & m = 0,2,4,6,\dots \end{cases} \end{aligned} \tag{4}$$

These conditions are referred to as odd- or even-moment conditions, depending on the value of m.

The commonly implemented S_N quadrature scheme, also referred to as level-symmetric quadrature [21], fully satisfies reflectional and rotational symmetries about all coordinate axes. The total number of directions for the S_N quadrature is $M = N(N+2)$, where N is an even integer. In the principal octant, the discrete directions are arranged on $N/2$ directional levels of constant polar angle (constant ξ), with $\frac{N}{2} - i + 1$ directions on the i^{th} level, where $i = 1,2,\dots,N/2$ [32]. Via symmetry, the directions in the principal octant can be easily mapped onto the remaining seven octants of the unit sphere. The S_N quadrature satisfies all even moment conditions ($m \geq 0$), as well as the first-order odd moment, for all direction cosines. Further details on the determination and derivation of this quadrature set are omitted, for brevity, but are readily available in literature [3,20].

While the S_N quadrature is commonly used for DOM simulation, it is limited in total direction number. For $N \geq 20$, satisfaction of moment conditions leads to physically unrealistic negative weighting factors [21]. This unrealistic behavior places an upper limit on the number of directions available for a given simulation. To combat this issue, several higher-order quadrature schemes were developed.

Longoni and Haghighat [31] proposed and developed both the Legendre-Equal Weight (P_N-EW) and Legendre-Chebyshev (P_N-T_N) quadrature sets. Determined using the Gauss-Legendre quadrature technique, these two quadrature sets have identical level arrangements and total number of directions to the S_N quadrature scheme. The major difference lies in the determination of the direction cosines and weighting factors. For both quadratures, the values of ξ_i in the principal octant,

which correspond to the i^{th} level of constant polar angle, are taken as the $N/2$ positive roots of $P_N(x)$, the N^{th}-order Legendre polynomial. The roots are taken such that $\xi_1 < \xi_2 < \cdots \xi_{N/2}$. The weighting factor w_i, which corresponds to a given direction on the i^{th} polar level, is taken thusly:

$$w_i = \frac{\pi}{\left(\frac{N}{2} - i + 1\right)(1-\xi_i^2)\left[\left(\frac{dP_N}{dx}\right)_{x=\xi_i}\right]^2} \tag{6}$$

where $i = 1, \ldots, N/2$ and $\frac{N}{2} - i + 1$ is the total number of equally-weighted directions on each polar level.

The difference between the two Legendre quadrature sets manifests in the determination of azimuthal angle for a given direction. For the P_N-T_N quadrature, azimuthal angles on each level are taken as the roots of the Chebyshev polynomials of the first kind. For the P_N-EW quadrature, azimuthal angles are determined using equal partitioning of the octant for a given polar angle. Thus, the azimuthal angles corresponding to the j^{th} direction on the i^{th} polar level are:

$$\phi_{i,j} = \begin{cases} \dfrac{j\pi}{2\left[\frac{N}{2} - i + 2\right]}, & P_N - EW \\ \dfrac{\pi[N + 3 - 2i - 2j]}{2[N + 2 - 2i]}, & P_N - T_N \end{cases} \tag{7}$$

where $i = 1, \ldots, N/2$ and $j = 1, \ldots, \frac{N}{2} - i + 1$. Both Legendre quadrature sets satisfy zeroth and first order moment conditions for all direction cosines. The P_N-EW satisfies even-moment conditions only for ξ due to the equipartitioning of azimuthal angle [31], while the use of Chebyshev polynomials for azimuthal angles in the P_N-T_N guarantees that all direction cosines satisfy even-moment conditions.

The Triangle Tessellation (T_N) [32] and Spherical Ring Approximation ($SRAP_N$) [33] quadratures were developed as specific alternatives to directionally restrictive quadrature sets. Both sets are completely geometric in construction, instead of relying on moment-matching. For the T_N quadrature set, the unit sphere surface is divided into $M = 8N^2$ continuous regions (N^2 per octant), $N \geq 1$. To construct the quadrature set, the principal octant is firstly mapped onto an equilateral basal triangle with vertices at (1,0,0), (0,1,0), and (0,0,1). Next, this triangle is tessellated into N^2 equilateral triangles, with side lengths equal to $1/N$ times the basal triangle length. Finally, the tessellated triangles are mapped onto the unit sphere. Direction cosines for the T_N quadrature are calculated as follows:

$$\mu = \frac{x_c}{\sqrt{x_c^2 + y_c^2 + z_c^2}}, \quad \eta = \frac{y_c}{\sqrt{x_c^2 + y_c^2 + z_c^2}}, \quad \xi = \frac{z_c}{\sqrt{x_c^2 + y_c^2 + z_c^2}} \tag{8}$$

where (x_c, y_c, z_c) is the coordinate locating the centroid of a single tessellated triangle in the basal plane. The weighting factors corresponding to a specific discrete direction are calculated as the area of the mapped spherical triangle through which the direction passes. Symmetry is applied to determine directions in the remaining octants.

For the $SRAP_N$ quadrature ($N \geq 2$), the surface of the unit sphere in the principal octant is subdivided into N spherical "rings", with the topmost "ring" reducing geometrically to a crown [33]. Working down from the crown element, each spherical ring is further divided into additional spherical elements. The number of divisions in successive rings forms an arithmetic progression, with the crown-shaped "ring" containing two spherical elements, and each successive ring containing an additional element. Using this approach, each spherical element will have an equal solid angle and elemental surface area. The discrete direction weights, which correspond to the elemental surface area, are thus equal for every discrete direction. The direction cosines for a given direction are determined by locating the centroid (x_c, y_c, z_c) of a given element, and then applying the transformation in Eq. (8). The total number of directions in the $SRAP_N$ quadrature, across all octants, is:

$$M = 8 * \left(2 + 3 + 4 + \cdots + (N+1)\right) = 8\sum_{i=2}^{N+1} i = 4N(N+3) \tag{9}$$

and the weighting factor for all discrete directions is $w = 4\pi/M$.

Both quadrature sets have been shown to accurately satisfy first-order moments [32,33]. While the T_N has been shown to be less accurate, in general, than the S_N quadrature of similar direction number, the absence of directional limit makes it more robust and flexible. It has also been shown that the T_N may suffer from numerical error, due to the fact that the discrete directions are calculated using centroids of tessellated triangles before unit sphere mapping. This mapping technique does not guarantee that the T_N directions pass directly through the elemental solid angle centroids. The $SRAP_N$ quadrature does not suffer from this shortcoming [33].

PHASE FUNCTION NORMALIZATION

After directional discretization of the continuous angular variation, overall scattered energy conservation should be maintained in the system. When scattering is anisotropic, satisfaction of the moment conditions of Eq. (4) is not sufficient to ensure energy conservation, and thus additional constraints are required. Phase-function normalization is a common technique to correct energy conservation errors, by which values of the scattered phase function are modified in order to satisfy the following scattered energy conservation condition:

$$\frac{1}{4\pi}\sum_{l=1}^{M} \tilde{\Phi}^{l'l} w^l = 1, \quad l' = 1, 2, \ldots, M \tag{10}$$

where $\tilde{\Phi}^{l'l}$ is the discrete value of normalized phase function. A simple technique that ensures satisfaction of Eq. (10) was presented by Kim and Lee [23]:

$$\tilde{\Phi}^{l'l} = \Phi^{l'l} * \left(\frac{1}{4\pi} \sum_{l=1}^{M} \Phi^{l'l} w^{l} \right)^{-1} \tag{11}$$

This technique has been shown to accurately conserve scattered energy in the system. However, recent works [25-30] have shown that this modification significantly distorts both the shape and asymmetry factor of the anisotropic scattering phase-function, leading to large errors in radiative transfer predictions. To correct this issue in order to maintain the original phase function scattering properties, an additional constraint must be satisfied after directional discretization and phase-function normalization, as follows [26]:

$$\frac{1}{4\pi} \sum_{l=1}^{M} \tilde{\Phi}^{l'l} \cos\Theta^{l'l} w^{l} = g, \qquad l' = 1, 2, \ldots, M \tag{12}$$

In order to obtain accurate radiative transfer solutions, both Eqs. (10) and (12) must be satisfied. When Eq. (12) is not completely satisfied, numerical error due to angular false scattering occurs [29,30]. Angular false scattering, which occurs solely due to angular discretization, is a second type of false scattering and should not be confused with traditional false scattering (numerical diffusion error brought on by spatial discretization).

Recently, Hunter and Guo [26-30] developed a phase-function normalization technique that accurately satisfies Eqs. (10) and (12) simultaneously. The phase function is normalized as follows:

$$\tilde{\Phi}^{l'l} = (1 + A^{l'l}) \Phi^{l'l} \tag{13}$$

Taking into account directional symmetry, the linear system of equations comprised of Eq. (13) and Eqs. (10) and (12) is underdetermined ($2M$ equations vs. $M(M+1)/2$ unknowns). The normalization parameters which accurately satisfy Eqs. (10) and (12) can be determined using the minimum-norm solution of this system, which is easily obtained using least-squares approximation or pseudo-inversion.

When applying Hunter and Guo's normalization technique, computational memory overflow can become an issue if inefficient storage is implemented. The coefficient matrix in this linear system contains $M^3 + M^2$ total elements. However, only $2M^2$ elements have a non-zero value, meaning that the total fraction of non-zero elements is on the order of M^{-1}. Use of a sparse coefficient matrix will maximize computational efficiency by storing only the non-zero terms in the matrix, reducing the memory load for this technique from $O(M^3)$ to $O(M^2)$.

Computational memory storage required for the normalization coefficient matrix is listed in Table 1 for both full and sparse matrix storage for various discrete direction numbers. In addition, the total percentage of non-zero elements is presented. For 24 total radiation directions, sparse storage of the coefficient matrix reduces total memory storage by 63.0% (due to the fact that only 8% of elements are non-zero). As the number of directions increase, computational memory overflow becomes a severe issue. For example, to store the coefficient matrix for M = 1680 discrete directions, over 35 GB of memory storage is required. Implementing sparse storage reduces the total memory requirement to 0.195 GB, reducing the necessary storage space by over 99%.

Table 1: Computational memory analysis of normalization parameter coefficient matrix in Hunter and Guo's normalization technique

N	M	% of Non-Zero	Coeff. Matrix Memory (GB)		% Savings w. Sparse
			Full	Sparse	
4	24	8.00	1.07E-04	3.97E-05	63.0
8	80	2.47	3.86E-03	4.41E-04	88.6
10	120	1.65	1.30E-02	9.93E-04	92.4
12	168	1.18	3.55E-02	1.95E-03	94.5
14	224	0.89	8.41E-02	3.46E-03	95.9
16	288	0.69	1.79E-01	5.72E-03	96.8
20	440	0.45	6.36E-01	1.33E-02	97.9
24	624	0.32	1.81E+00	2.68E-02	98.5
28	840	0.24	4.42E+00	4.86E-02	98.9
32	1088	0.18	9.60E+00	8.16E-02	99.2
36	1368	0.15	1.91E+01	1.29E-01	99.3
40	1680	0.12	3.53E+01	1.95E-01	99.4
44	2024	0.10	6.18E+01	2.82E-01	99.5
52	2808	0.07	1.65E+02	5.43E-01	99.7
64	4224	0.05	5.62E+02	1.23E+00	99.8

Application of scattered energy normalization only (Eq. (11)) is guaranteed to explicitly conserve system scattered energy, but may result in angular false scattering. It is important, therefore, to examine the magnitude of angular false scattering due to asymmetry factor distortion after application of Eq. (11). Overall change in scattering effect, due to distortion in asymmetry factor g, is manifested in the difference of $(1-g)$, according to the isotropic scaling law [35,36]. By investigating the difference in $(1-g)$ after application of Eq. (11), additional information about the necessity of conserving overall asymmetry factor can be determined.

The percent difference in $(1-g)$ after application of Eq. (11) only for the five previously discussed quadrature sets versus discrete direction number is shown in Figure 2. An HG phase function with g = 0.9300 is specified before angular discretization. As seen in the figure, all quadrature sets exhibit a similar behavior, with increases in direction number producing large decreases in scattering effect change. For the lowest-order quadratures, deviations of >90% are witnessed for all five quadrature schemes. At the S_N directional limit (S_{16}), a 44.1% change in scattering effect is witnessed, illustrating the shortcomings of a set upper directional limit. Changes in

scattering effect of less than 10% are first realized around M = 1000 for the four higher-order quadratures.

At greater direction numbers ($M \approx 2000$), percent differences are on the order of 2-3% for all quadratures, indicating that error due to angular false scattering may still exist in radiative transfer predictions at such high direction number. All four higher-order quadratures exhibit similar behavior, although changes for P_N-T_N and $SRAP_N$ are smallest. Substantial increases in direction number result in the percent scattering effect change converging towards zero, demonstrating a potential advantage of non-limited quadrature sets. However, to effectively minimize scattering effect changes after application of Eq. (11), extremely fine angular grids must be implemented, which greatly impacts computational efficiency. When Hunter and Guo's technique is applied, and Eq. (12) is satisfied, no change in scattering effect exists.

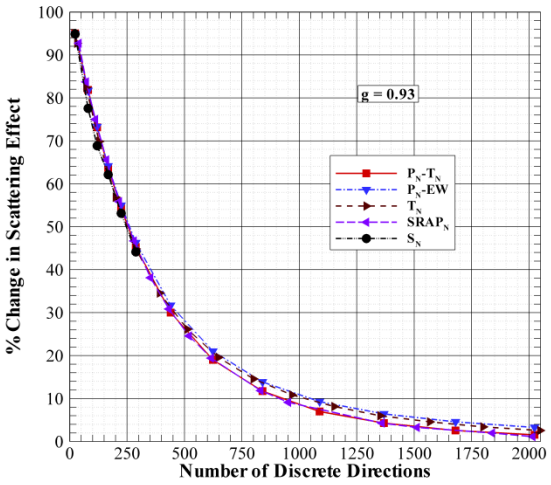

Fig. 1: Percent change in scattering effect vs. number of discrete directions for various DOM quadrature schemes after implementing scattered energy conservation of Eq. (11)

RESULTS AND DISCUSSION

Figure 1 gives a rudimentary indication of the impact of improper phase-function normalization on DOM solutions using higher-order quadrature sets. It is necessary, however, to examine the direct impact of phase-function normalization and angular false scattering on actual radiative transfer predictions, determined using higher-order quadrature, to further resolve a conclusion.

The benchmark test problem for this analysis involves steady-state radiative transfer in a 3-D cubic, enclosure with edge length L, which houses an optically thick ($\tau = (\sigma_a + \sigma_s)L = 10.0$), purely scattering ($\omega = 1.0$) medium that scatters radiant energy anisotropically with g = 0.93. Spatial coordinate non-dimensionalization is applied as follows:$x^* = x/L$, $y^* = y/L$, and $z^* = z/L$. As a further simplification, the edge length of the cube is taken as unity. The spatial grid for all simulations is taken as $(N_x \text{ x } N_y \text{ x } N_z) = 27 \text{ x } 27 \text{ x } 27$ to ensure radiative transfer prediction invariance with further refinement. The wall at $z^* = 0$ is taken to be a diffuse blackbody emitter, with unity emissive power. The remaining walls and medium are taken as cold and black. The positive differencing scheme [3] is applied. All simulations were performed on a Dell Optiplex 780, with 4.0 GB of RAM and an Intel Core 2 processor. Radiative transfer solutions using the DOM are generated using the FORTRAN language, while the normalization parameters of Hunter and Guo's technique are determined using MATLAB's built-in least-squares solver.

Figure 2(a-b) compares radiative heat flux determined using the DOM with various quadrature sets to a reference Monte Carlo solution [25], in order to gauge the impact of both phase-function normalization and DOM quadrature on radiative transfer predictions. Radiative heat fluxes are calculated at the centerline of the wall opposite from the diffuse source, i.e. $Q(x^*, y^* = 0.5, z^* = 1.0)$ and presented against location x^*. The reference MC solution of Boulet et al. [25] implements greater than 4 million quanta per reference control volume. The DOM solutions are presented using both scattered energy normalization and Hunter and Guo's normalization for all five quadrature sets.

Radiative heat fluxes are presented for DOM quadrature with discrete direction number on the order of the S_4 quadrature ($M = 24$) in Figure 2(a), with the T_2 ($M = 32$ and $SRAP_2$ ($M = 40$) chosen since their direction numbers are the closest possible. Using scattered energy normalization only, generated heat flux profiles differ greatly from the reference MC solution for all quadratures. The maximum percentage differences with respect to MC for S_4, P_4-EW, P_4-T_4, T_2, and $SRAP_2$ are 222%, 111%, 110%, 131%, and 68.8%, respectively. The heat flux profile generated with $SRAP_2$ is physically incorrect in shape, as the highest heat flux should occur at $x^* = 0.50$ (furthest away from the cold wall boundary). Application of Hunter and Guo's technique conserves asymmetry factor after directional discretization, and causes a substantial decrease in the difference between DOM and MC heat flux profiles. The maximum differences for the five quadratures decrease to 92.9%, 18.9%, 16.7%, 41.1%, and 23.8%, respectively. While improvement is seen, errors due to ray effect still strongly manifest due to the weak approximation of the continuous angular variation. It is also noteworthy to mention that all four high-order quadrature sets predict more closely to the MC than the S_N quadrature, regardless of normalization, indicating their potential as accurate alternatives to the S_N quadrature for lower direction number.

Figure 2(b) depicts radiative heat fluxes determined using DOM quadratures on the order of the S_8 quadrature (M = 80). In comparison to Figure 2(a), it is seen that increase in direction number dramatically reduces the discrepancy between DOM and MC reference solutions, although significant errors are still witnessed when scattered energy normalization is applied. Differences for the five quadratures range between 48-75% due to angular false scattering. Application of Hunter and Guo's

technique results in a dramatic improvement, with all five quadrature sets producing heat fluxes within 10% of the MC reference solution at all x^*. This indicates that the increase in direction number has more effectively mitigated errors due to ray effect, while the normalization approach has mitigated angular false scattering error.

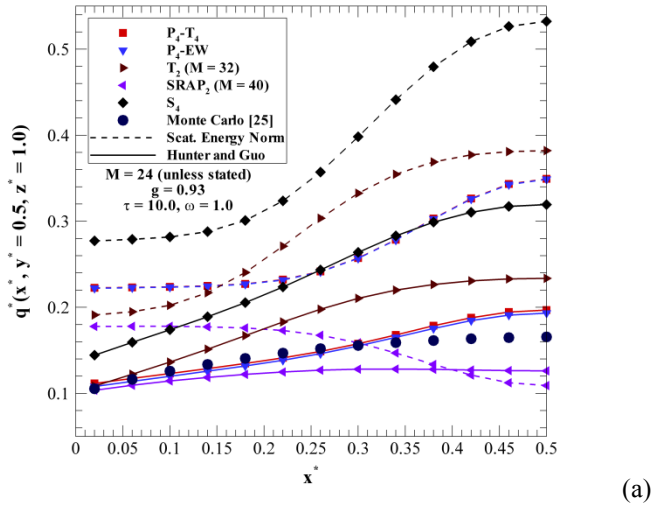

(a)

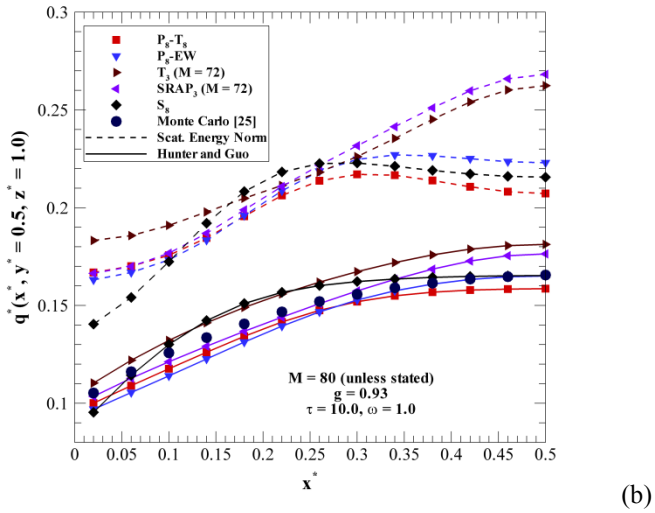

(b)

Fig. 2: Comparison of Q(x*, y* = 0.5, z* = 1) for diffuse heating at z* = 0 wall between MC solutions [25] and DOM solutions using various quadrature schemes with a) S_4 and b) S_8 equivalent quadrature

Figure 3 plots the percent difference in heat flux from the reference MC solution vs. x^* for the five DOM quadratures using S_{12} equivalent quadrature ($M = 168$). The percentage differences shown in this figure are calculated as $\frac{Q_{DOM}-Q_{MC}}{Q_{MC}} \times 100\%$, so that the sign indicates heat flux over- or under-predictions. The T_5 ($M = 200$) and $SRAP_5$ ($M = 160$) quadratures are shown in this figure, as their direction numbers are the closest available to the S_{12} direction number.

When scattered energy normalization of Eq. (11) is applied, all five quadratures significantly overpredict the MC solution for all locations. The maximum differences range between 30.0% for the T_5 quadrature to 42.0% for the S_{12} quadrature. More accurate agreement of the T_5 quadrature over the remaining four sets is expected, as the direction number of $M = 200$ is significantly higher. In general, MC and DOM heat flux differences decrease with increasing x^*. The profile generated using the S_{12} quadrature is similar to those produced by P_{12}-T_{12} and $SRAP_5$ near $x^* = 0$ and $x^* = 0.5$, but differs greatly in between. Similarly, the two Legendre quadratures exhibit nearly identical behavior near the cold wall at $x^* = 0$, but display different behavior with increasing x^*.

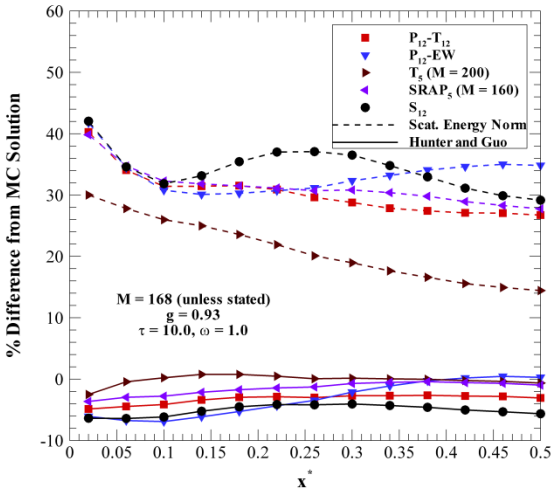

Fig. 3: Percent difference in Q(x*, y* = 0.5, z* = 1) for diffuse heating at z* = 0 wall between MC solutions [25] and DOM solutions using various quadrature schemes with a) S_{12} equivalent quadrature

Application of Hunter and Guo's technique reduces the discrepancy between DOM and MC heat fluxes to less than 7% for all quadratures. DOM heat fluxes underpredict the MC value at all locations, except for a small range of x^* for the T_5 quadrature. On average, the S_{12} quadrature is the least accurate (average underprediction of 5.1%), while the T_5 is the most accurate (average underprediction of 0.1%). Similar results are witnessed when quadratures on the order of S_{16} ($M = 288$) are examined, although the results are not shown here due to space considerations. When scattered energy normalization is applied, the percent differences between DOM and MC range between 22.4% for the T_6 quadrature to 35.9% for the S_{16} quadrature. Application of Hunter and Guo's technique reduces the differences to less than 6% in absolute value for all quadratures, with average differences ranging between -0.56% for $SRAP_7$ and -3.00% for P_{16}-T_{16}. Errors of such magnitude, as witnessed for S_{12} and S_{16} equivalent quadratures, are

generally considered acceptable, due to statistical errors inherent in the MC method and discretization errors inherent in the DOM.

The results in Figures 2(a-b) and 3 follow the expected trend from the analysis of scattering effect change in Figure 1. Direction number increases tend to reduce angular false scattering errors, leading to DOM heat flux profiles that are more accurate in comparison with MC when only scattered energy normalization is applied. However, significant errors still exist for all S_{16} quadrature sets when Eq. (11) is implemented, corresponding to the ~40% change in scattering effect seen in Figure 2 for quadratures of this order. While the higher-order quadratures conform to MC with equal or greater accuracy than the S_N quadrature, angular false scattering errors still abound. Hunter and Guo's technique has been shown to effectively minimize angular false scattering and improve DOM solution accuracy, with errors > 10% only witnessed for the lowest-order quadrature due to ray effect.

One method of effectively reducing errors due to ray effect and angular false scattering is to further refine the angular grid by increasing discrete direction number. Figures 4(a-b) examine the percent difference in heat flux between the DOM and reference MC solutions vs. discrete direction number at two different locations: near the cold wall at $x^* = 0.02$, and at the wall center ($x^* = 0.50$), respectively. DOM heat fluxes are generated using the four higher-order quadrature sets using either scattered energy normalization only or Hunter and Guo's normalization technique.

At $x^* = 0.02$ (Figure 4(a)), discrepancies between MC and DOM heat fluxes decreases with an increase in direction number for all quadratures, corresponding to the decrease in scattering effect change witnessed in Figure 1. An important note, however, is that these discrepancies do not converge to zero, meaning that the DOM solution does not converge directly to the MC solution. Instead, the percent differences converge to a slightly negative percentage due to the inherent statistical and numerical errors in the two solution schemes. As an example, the percent differences between DOM and MC heat fluxes for the P_{44}-T_{44} (M = 2024), P_{44}-EW (M = 2024), T_{16} (M = 2048), and $SRAP_{21}$ (M = 2016) quadratures reach values of -1.26%, -0.19%, -1.41%, and -1.60%, respectively. Application of between M = 750 and 1000 directions should be applied to obtain heat fluxes that differ by less than 5% at this location, depending on chosen quadrature scheme, when scattered energy normalization is applied.

Application of Hunter and Guo's technique results in absolute differences of less than 5% for all quadratures except P_N-EW when M = 288. Increase in discrete direction number does not appear to substantially impact heat fluxes generated using Hunter and Guo's technique. Over the range of discrete directions shown in Figure 4(a), the percent differences only improve by 0.94%, 1.08%, 0.07%, and 0.66% for the P_N-T_N, P_N-EW, T_N, and $SRAP_N$ quadratures, respectively, indicating that higher-order directionality might be unnecessary if asymmetry factor is already accurately conserved after angular discretization.

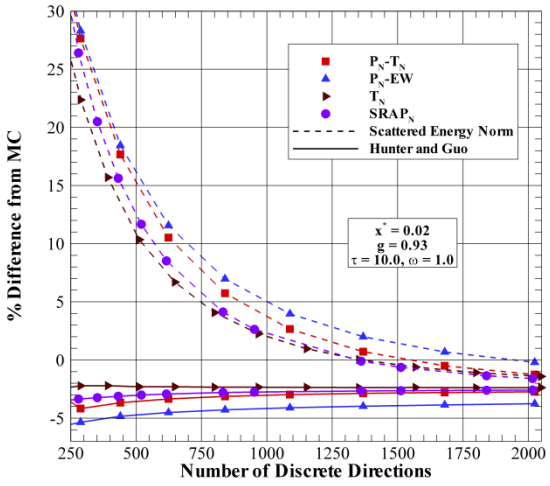

(a)

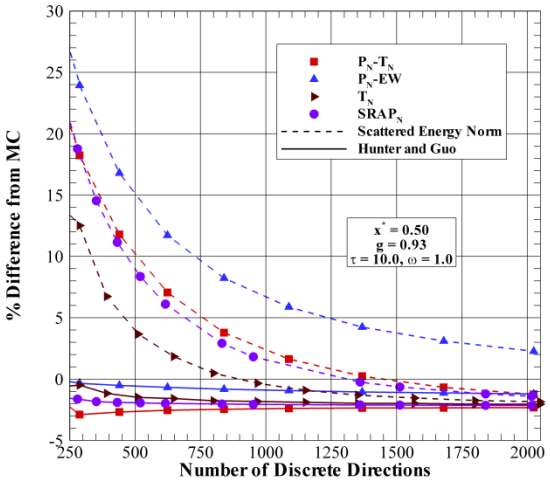

(b)

Fig. 4: Percent difference in Q(x*, y* = 0.5, z* = 1) between MC solution [25] and DOM solutions vs. number of discrete directions for various DOM quadrature sets at a) x* = 0.02 and b) x* = 0.50

Similar results are witnessed at $x^* = 0.50$ in Figure 4(b). Discrepancies between the four quadrature sets when scattered energy normalization is applied are more prominent than seen in Figure 4(a). Heat fluxes generated with the P_N-EW quadrature more greatly overpredict the MC solution than the three remaining quadratures over the entire directional range analyzed. In addition, while the three remaining quadratures have begun to underpredict the MC solution, these heat fluxes continue to overpredict, indicating a slower convergence rate. The total number of directions required for the P_N-EW to attain a percentage difference of less than 5% at this location is M = 1368, while the remaining quadratures require M = 840 or fewer discrete directions. A similar trend to Figure 4(a) is witnessed when Hunter and Guo's technique is applied, as

differences of less than 3% are witnessed for all quadratures across the entire directional range analyzed, with only minimal improvement witnessed with increase in direction number. For both locations, it appears that heat fluxes generated with scattered energy normalization and Hunter and Guo's technique converge to similar steady-state values (as judged by the convergence of the percentage difference profiles), but Hunter and Guo's technique converges with fewer directions.

The advent of higher-order quadrature sets provides a possible alternative to phase-function normalization. Hunter and Guo's normalization was shown to be necessary for highly anisotropic scattering at lower direction number, due to deviations in both scattered energy and asymmetry factor conservation caused by a poorly-refined angular grid. The possibility exists, however, that with sufficiently large discrete direction number, scattered energy and asymmetry factor may be accurately conserved without additional phase-function normalization required. This hypothesis is investigated in Figure 6, in which DOM heat flux profiles generated using the P_N-T_N quadrature with extremely high direction numbers and no additional phase-function normalization are compared to the reference MC solution. Heat fluxes are generated using the P_{44}-T_{44} (M = 2024), P_{52}-T_{52} (M = 2808), and P_{64}-T_{64} (M = 4224) quadratures, respectively. Use of lower direction numbers without normalization is impossible, as divergent radiative heat flux profiles are attained due to lack of scattered energy conservation.

As direction number increases, converging trends are witnessed for the DOM heat flux profiles. Differences from MC of between 27-30% are witnessed for the P_{44}-T_{44} quadrature, corresponding to a 21.9% change in scattering effect due to the distortion of asymmetry factor to a discretized value of g = 0.9453. This indicates that the angular grid is still too coarse to obtain an accurate solution. Increase of direction number to M = 2808 for the P_{52}-T_{52} quadrature reduces discrepancies between DOM and MC to less than 10% for all locations, as the discretized value of g reduces to 0.9356 for this situation. For the extreme case (P_{64}-T_{64}), the differences are less than 1.4% for all locations, corresponding to a 1.9% change in scattering effect (discretized g = 0.9313), indicating that some angular false scattering is still present, although minimal. For comparison, if Eq. (11) is applied, and scattered energy normalization is implemented, the discretized g for this quadrature reduces to g = 0.9301, corresponding to a 0.14% scattering effect change. This profile underpredicts the MC solution by less than 2.5% at all locations, which conforms to the expected results from Figures 4(a-b).

Although the results show that higher-order DOM quadratures are able to minimize angular false scattering errors effectively, they do so with a major cost to computational efficiency. Increases in discrete direction number directly result in increases in both computational time (due to increased number of flops) and computational committed memory (due to increasing array sizes).

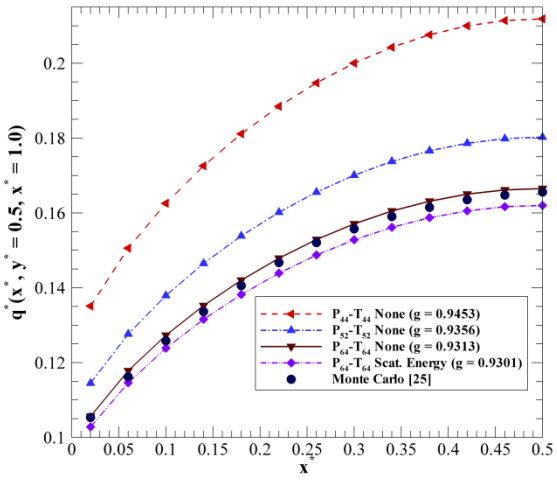

Fig. 5: Comparison of Q(x*, y* = 0.5, z* = 1.0) for diffuse heating at z* = 0 wall between MC solutions [25] and DOM solutions using extremely high-order P_N-T_N quadrature without phase-function normalization

Figure 6 examines computational convergence times, in minutes, versus the total number of discrete directions for various quadrature sets. At low direction number, all five sets converge in similar amounts of time, with total convergence time of ~12 minutes seen for S_{16} equivalent quadratures. Convergence time dramatically increases, in a non-linear fashion, with increase in discrete direction numbers. Convergence times for the P_N-T_N quadratures with M = 624, 840, 1368, and 2024 discrete directions are 98, 195, 557, and 1330 minutes, respectively. Although it is not presented in Figure 6, the computational time required for obtaining the non-normalized P_{64}-T_{64} solution in Figure 5 was 7107 minutes, or 4.94 days. Convergence times on this order are extremely impractical, and illustrate a major issue with using such higher-order quadratures to eliminate angular false scattering and obtain accurate radiative transfer solutions.

Generally, it appears more practical and efficient to implement Hunter and Guo's normalization technique to conserve scattered energy and asymmetry factor, as accurate solutions are obtained with far fewer directions necessary. As an example, in Figures 4(a-b), achieving a percent difference of 6% or less at all locations required 840 discrete directions for the P_N=T_N quadrature using scattered energy normalization, but Hunter and Guo's technique reduced the necessary number of directions to 168 in order to obtain such accuracy. This reduction in direction number from 840 to 168 reduces the computational time requirement by 98%, from ~195 minutes to 4 minutes, without loss of solution accuracy.

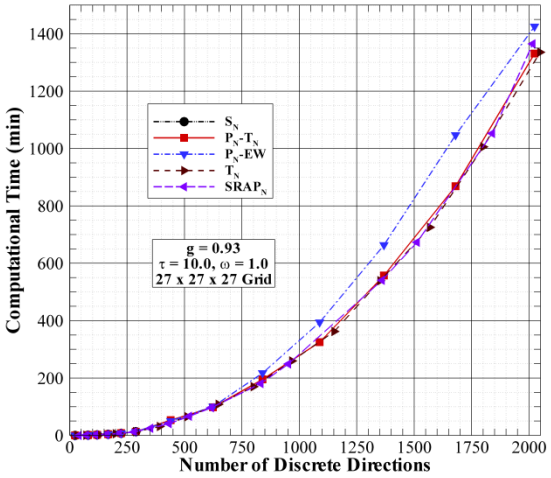

Fig. 6: DOM computational time vs. number of discrete directions for various DOM quadrature schemes

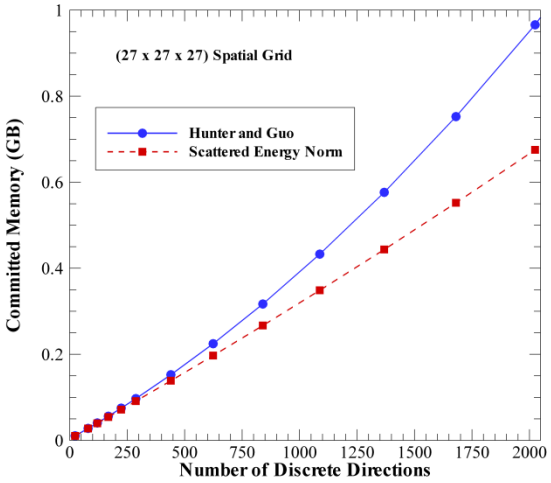

Fig. 7: Comparison of computational memory vs. number of discrete radiation directions with Hunter and Guo's normalization technique and scattered energy normalization

Figure 7 examines the total computational memory commitment (determined through the operating system) for the DOM when either scattered energy normalization or Hunter and Guo's technique is applied. Computational memory is independent of the quadrature scheme apart from the total number of discrete directions. At low direction number, the computational memory requirement for each normalization technique is on the same order. Increase in direction number causes a separation between the two memory requirements, as Hunter and Guo's technique requires storage of the $O(M^2)$ normalization coefficient matrix. While Hunter and Guo's technique does require more memory than scattered energy normalization at similar direction number, it was shown in Figures 4(a-b) that an increase in direction number using Hunter and Guo's technique did not drastically improve solution accuracy. Using the example illustrated for Figure 6, n order to achieve solution accuracy of <6% at all locations when compared to MC, 840 and 168 directions are required for the two techniques, respectively. The reduction in directions using Hunter and Guo's technique results in a computational memory reduction of 78.9% (0.27 GB to 0.06 GB).

CONCLUSION

The use of higher-order DOM quadrature schemes to accurately calculate radiative transfer in highly anisotropic media, as well as the manifestation of angular false scattering with higher-order quadratures and phase-function normalization techniques, is investigated in this study.

For low direction numbers ($M \leq 288$), higher-order quadrature schemes produce heat fluxes that are as accurate or even more accurate when compared to MC as the directionally-limited S_N quadrature. Additionally, all quadratures suffer from angular false scattering when scattered energy normalization is applied, due to a lack of phase-function asymmetry factor conservation. While substantial increases in direction number are shown to effectively minimize angular false scattering and ray effect for all higher-order schemes, dramatic increases in both computational convergence time and memory requirements are major consequences of this approach, reducing the overall practicality of such a strategy. Hunter and Guo's normalization technique is shown to effectively minimize angular false scattering for all direction numbers, as well as producing heat flux profiles that conform accurately to MC solutions for all quadratures and direction numbers except the very lowest order ($M = 24$), where ray effect predominates. Further increase in direction number only provides minimal improvement to DOM heat fluxes for this technique.

Application of Hunter and Guo's normalization technique is a practical and efficient method for determining radiative transfer in highly anisotropic scattering media, due to substantial reductions in computational time and memory over both scattered energy normalization and use of extremely high direction numbers to counteract angular false scattering errors.

REFERENCES

[1] Chadrasekhar, S., 1990, *Radiative Transfer,* Dover Publications, 1960.

[2] Lathrop, K.D., 1966, "Use of discrete-ordinate methods for solution of photon transport problems", Nuc. Sci. Eng., 24, pp. 381-388.

[3] Modest, M.F., 2003, *Radiative Heat Transfer*, *2nd ed.,* Academic Press, New York, pp. 263-284, 498-530.

[4] Carlson, B.G., and Lathrop, K.D., 1968, "Transport theory- the method of discrete-ordinates", in Greenspan, H., Kelber, C.N., Okrent, D. (eds.), *Computing Methods in Reactor Physics*, Gorden and Breach, New York.

[5] Guo, Z., Maruyama, S., and Tagaway, S., 1998, "Combined heat transfer in floating zone growth of large

silicon crystals with radiation on diffuse and specular surfaces", J. Crystal Growth, 194, pp. 321-330.

[6] Guo, Z., and Maruyama, S., 2000, "Radiative heat transfer in nonhomogeneous, nongray, and anisotropic scattering media", Int. J. Heat Mass Transf., 43, pp. 2325-2336.

[7] Solovjov, V.P., and Webb, B.W., 2001, "An efficient method for modeling radiative transfer in multicomponent gas mixtures with soot", J. Heat Transfer, 123, pp. 450-457.

[8] Tuncer, O., Acharya, S., and Uhm, J.H., 2009, "NO_x and flashback characteristics of confined premixed hydrogen-enriched methane flames", Int. J. Hydrogen Energy, 34, pp. 496-506.

[9] Yamada, Y., 1995, "Light-tissue interaction and optical imaging in biomedicine", Annu. Rev. Heat Transfer, 6, pp. 1-59.

[10] Mitra, K., and Kumar, S., 1999, "Development and comparison of models for light-pulse transport through scattering-absorbing media", App. Optics, 38, 188-196.

[11] Kim, K.H., and Guo, Z., 2004, "Ultrafast radiation heat transfer in laser tissue welding and soldering", Num. Heat Transfer A, 46, pp. 23-40.

[12] Kim, K.H., and Guo, Z., 2007, "Multi-time-scale heat transfer modeling of turbid tissues exposed to short-pulsed irradiations", Comp. Meth. Prog. Bio., 86, pp. 112-123.

[13] Jaunich M., Raje, S., Kim, K.H., Mitra, K., and Guo, Z., 2008, "Bio-heat transfer analysis during short pulse laser irradiation of tissues", Int. J. Heat Mass Transfer, 51, pp. 5511-5521.

[14] Fiveland, W.A., 1984, "Discrete-ordinates solutions of the radiative transport equation for rectangular enclosures", J. Heat Transfer, 106, pp. 699-706.

[15] Fiveland, W.A., 1988, "Three dimensional radiative heat transfer solution by the discrete-ordinates method", J. Thermophys. Heat Transfer, 2, pp. 309-316.

[16] Truelove, J.S., 1988, "Three-dimensional radiation in absorbing-emitting-scattering media using the discrete ordinates approximation", J. Quant. Spectrosc. Radiat. Transfer, 39, pp. 27-31.

[17] Guo, Z., and Kumar, S., 2001, "Discrete-ordinates solution of short-pulsed laser transport in two-dimensional turbid media", Appl. Optics, 40, pp. 3156-3163.

[18] Guo, Z., and Kumar, S., 2002, "Three-dimensional discrete ordinates method in transient radiative transfer", J. Thermophys. Heat Transfer, 16, pp. 289-296.

[19] Akamatsu, M., and Guo, Z., "Ultrafast radiative heat transfer in three-dimensional highly-scattering media subjected to pulse train irradiation", Num. Heat Transf. A, 59(9), 653-671.

[20] Fiveland, W., 1991, "The selection of discrete ordinates quadrature sets for anisotropic scattering", Fund. Rad. Heat Transfer ASME-HTD, 160.

[21] Endo, T., and Yamamoto, A., 2007, "Development of new solid angle quadrature sets to satisfy even- and odd-moment conditions", J. Nuc. Sci. Tech., 44(10), pp. 1249-1258.

[22] Chai, J.C., Lee, H.O., and Patankar, S.V., 1993, "Ray effect and false scattering in the discrete ordinates method", Num. Heat Transfer B, 24, pp. 373-389.

[23] Kim, T.K., and Lee, H., 1988, "Effect of anisotropic scattering on radiative heat transfer in two-dimensional rectangular enclosures", Int. J. Heat Mass Transfer, 31, pp. 1711-1721.

[24] Wiscombe, W.J., 1976, "On initialization, error and flux conservation in the doubling method", J. Quant. Spectrosc. Radiat. Transfer, 16, pp. 637-658.

[25] Boulet, P., Collin, A., and Consalvi, J.L., 2007, "On the finite volume method and the discrete ordinates method regarding radiative heat transfer in acute forward anisotropic scattering media", J. Quant/ Spectrosc. Radiat. Transfer, 104 (1), pp. 460-473.

[26] Hunter, B., and Guo, Z., 2012, "Conservation of asymmetry factor in phase function normalization for radiative transfer analysis in anisotropic scattering media", Int. J. Heat Mass Transfer, 55, 1544-1552.

[27] Hunter, B., and Guo, Z., 2012, "Reduction of angle splitting and computational time for the finite volume method in radiative transfer analysis via phase function normalization", Int. J. Heat Mass Transfer, 55, pp. 2449-2460.

[28] Hunter, B., and Guo, Z., 2012, "Phase function normalization for accurate analysis of ultrafast collimated radiative transfer", Appl. Optics, 51, pp. 2192-2201.

[29] Hunter, B., and Guo, Z., 2012, "Phase-function normalization in 3-D discrete-ordinates solution of radiative transfer – Part I: Conservation of scattered energy and asymmetry factor", Num. Heat Transfer B, 62, pp. 203-222.

[30] Hunter, B., and Guo, Z., 2012, "Phase-function normalization in 3-D discrete-ordinates solution of radiative transfer – Part II: Benchmark comparisons", Num. Heat Transfer B, 62, pp. 223-242.

[31] Longoni, G., and Haghighat, A., 2001, "Development of new quadrature sets with the "ordinate splitting" technique", Proc. of 001 ANS Int. Meeting on Mathematical Methods for Nuclear Applications, Salt Lake City, Utah, Sept. 9-13, 2001.

[32] Thurgood, C.P., Pollard, A., and Becker, H.A., 1995, "The T_N quadrature set for the discrete ordinates method", J. Heat Transfer, 117, pp. 1068-1070.

[33] Li, B-W., Yao, Q., Cao, X-Y., and Cen, K-F., 1998, "A new discrete ordinates quadrature scheme for three-dimensional radiative heat transfer", J. Heat Transfer, 120, pp. 514-518.

[34] Chai, J.C., Lee, H.S., and Patankar, S.V., 1998, "Improved treatment of scattering using the discrete ordinates method", J. Thermophys. Heat Transfer, 12, pp. 605-608.

[35] Guo, Z., and Maruyama, S., 1999, "Scaling anisotropic scattering in radiative transfer in three-dimensional nonhomogeneous media", Int. Comm. Heat Mass Transfer, 26, pp. 997-1007.

[36] Lee, H., and Buckius, R.O., 1982, "Scaling anisotropic scattering in radiation heat transfer for a planar medium", J. Heat Transf., 104, pp. 68-75.

